# Two topics
# on temporal and spectral variations
# of X-ray sources

Hajime Inoue
Institute of Space and Astronautical Science, JAXA

・Origin of super-orbital periodicities of binary X-ray sources

- Preccessions of accretion disks in close binaries

・Origin of erratic X-ray variation and seemingly broad iron line spectral feature in Seyfert galaxies

- A variable partial covering with absorbers over the central X-ray source

# A preccession of the accretion disk

**Her X-1**

X-ray pulsar period 1.24 sec

close binary period 1.7 days

X-ray on-off period ~ 35 days

⇩

a preccession of the accretion disk

X-ray flux

(Jones & Forman 1976)

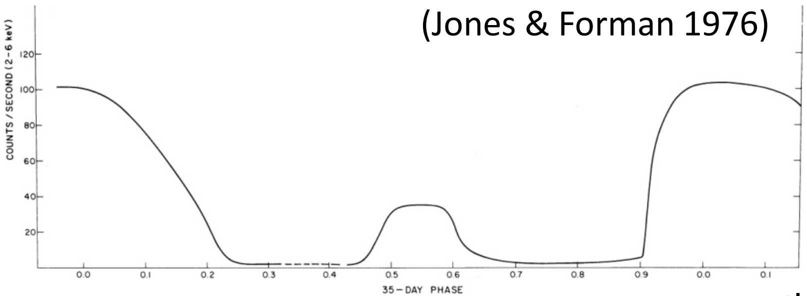


time

35 days

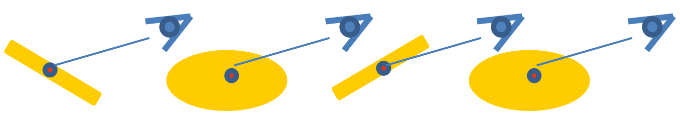

(Giacconi et al. 1973)

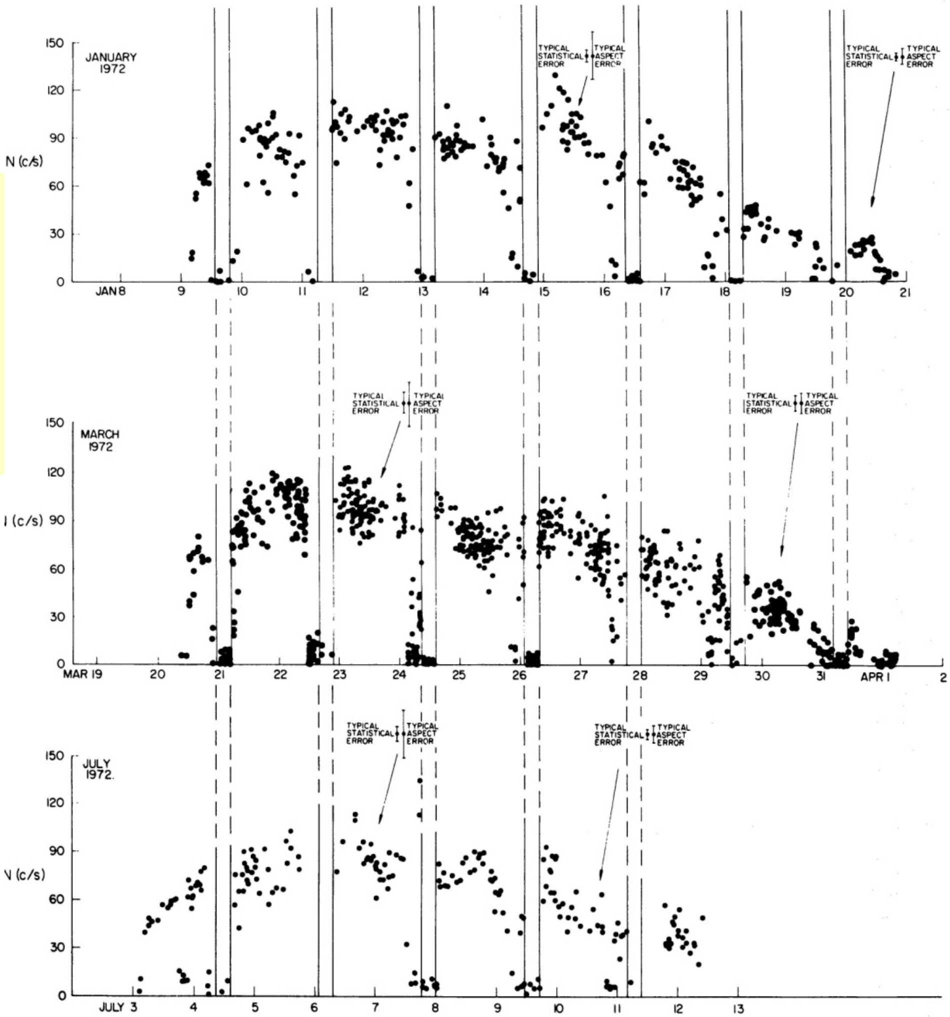


FIG. 2.—Hercules intensity data (2–6 keV) during three ON states. The vertical lines represent the orbital eclipses, whose positions are determined accurately from the pulsation Doppler analysis. Typical errors appropriate for different groups of data are shown; the statistical error bar is relevant for point-to-point comparisons, and the aspect error bar is relevant for day-to-day comparisons. It should be noted that most intensity points below about 10 counts $s^{-1}$ are upper limits.

# SS433

close binary period 13.1 days

Relativistic jets
velocity ～0.26 C
preccession tilt angle ～20°
period ～162.5 days

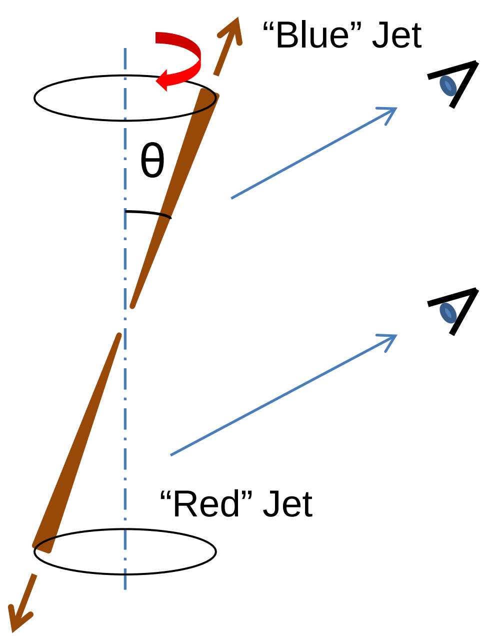


(Margon 1984)

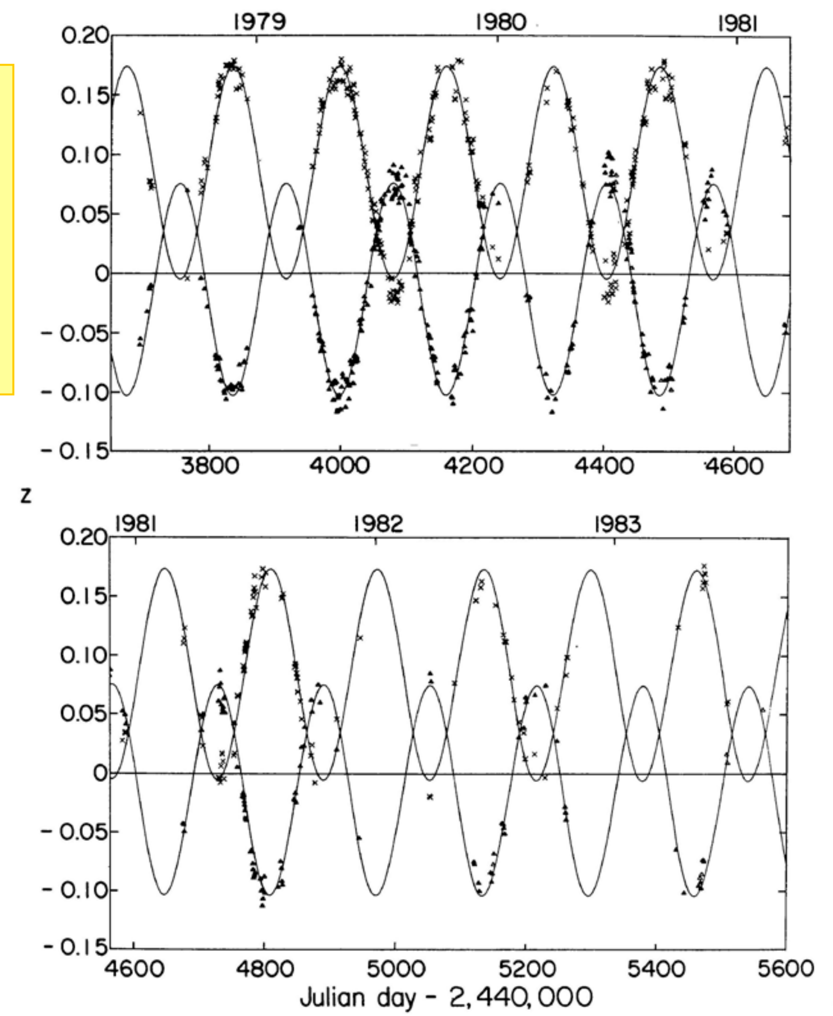


*Figure 1* Doppler shifts of SS 433 on 450 nights in the period 1978–83. The majority of these data were obtained by the author and colleagues, supplemented by sources cited in (105). The solid curve is a least-squares best fit to the simple "kinematic model" (1). The free parameter values and their associated 1$\sigma$ uncertainties (notation as in 105) for this fit are $v/c = 0.2601 \pm 0.0014$, $\theta = 19.80° \pm 0.18°$, $i = 78.82° \pm 0.11°$, $t_0 =$ JD 2,443,562.27 $\pm$ 0.39, $P = 162.532 \pm 0.062$ days.

a preccession of the accretion disk ?

# A preccession of an accretion disk induced by the tidal force from the companion star

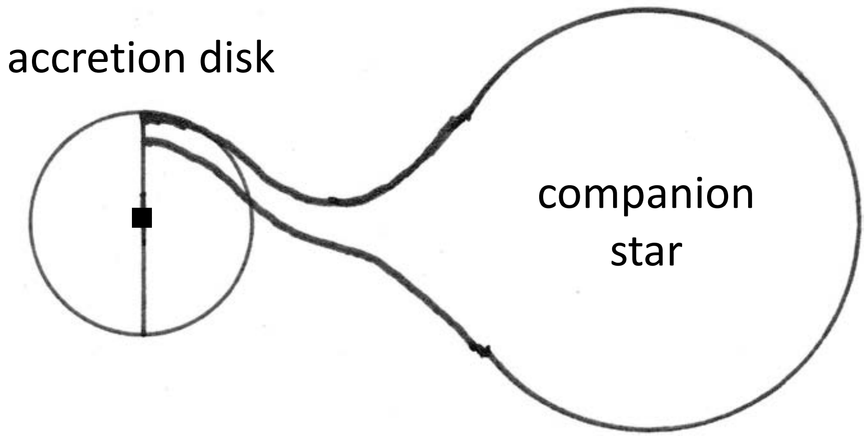


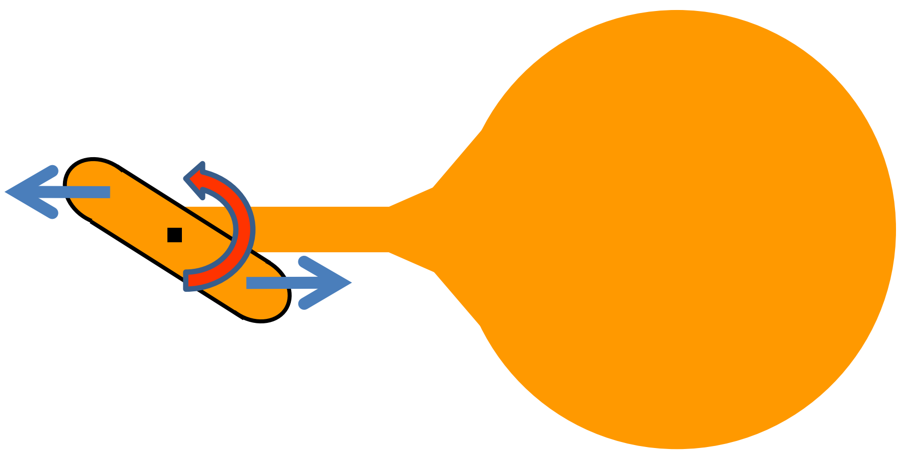

When the accretion disk tilts, the tidal force from the companion star induces a torque on it.

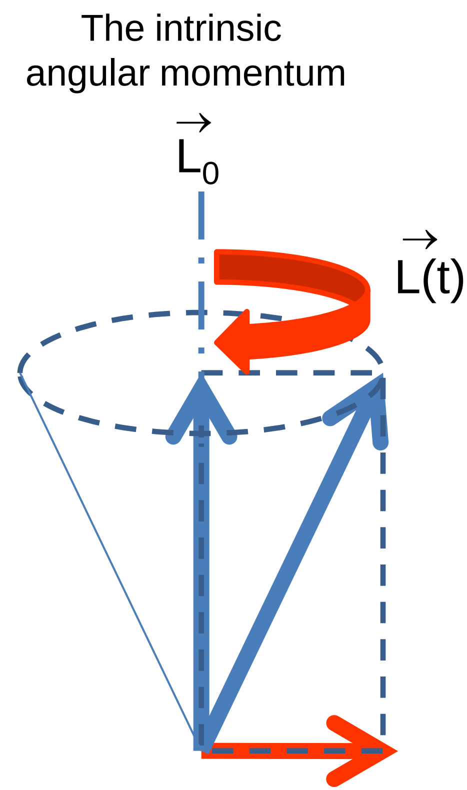


The torque causes a preccession of the disk.

When all the fluid particles have the same angular momentum per mass around the compact star,

$$l = (RGM_X)^{1/2},$$

a ring is formed with the average radius, R and the average angular velocity,

$$\Omega = \frac{(GM_X)^{1/2}}{R^3} .$$

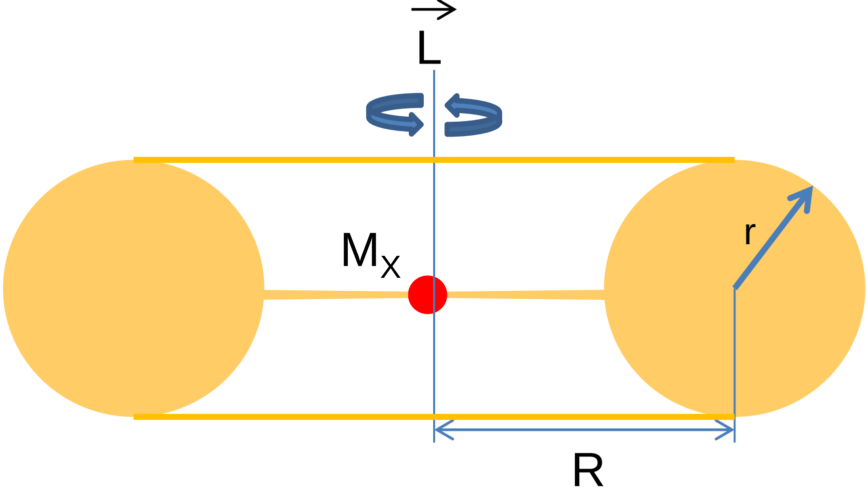


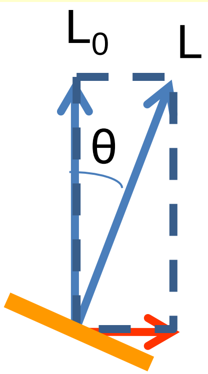


The total angular momentum of the ring, L, is

$$L = M_R\, R^2\, \Omega \propto R^{1/2}.$$ ($M_R$: the ring mass)

When the angular momentum axis tilts from the intrinsic axis by an angle, $\theta$,

$$L = L_0 \cos^{-1}\theta .$$

(Subscript 0 indicates parameters without tilt)

⇨ $R = R_0 \cos^{-2}\theta$

When the tilt angle $\theta$ ↗ , the ring radius R ↗.

Hydrostatic balance in the meridian cross section of the ring

$$\frac{dP}{dr} = -\rho \frac{GM_X}{R^3}\, r$$

⇩

On an iso-thermal approximation,

$$\rho \propto \exp[- r^2 / 2\, a^2 ],$$

where $a = \left[ \dfrac{kTR^3}{\mu m_H G M_X} \right]^{1/2} \propto T^{1/2} R^{3/2}$ .

Adiabatic expansion of the ring

$$T/T_0 = (V/V_0)^{-2/3}$$

$$V \propto Ra^2$$

$$T/T_0 = (R/R_0)^{-8/5} \propto \cos^{16/5}\theta$$

When the tilt angle $\theta$ ↗, the ring temperature T ↘.

# The energetics of the ring as a function of the tilt angle

- rotational energy

$E_K = (1/2)\, M_R\, R^2\, \Omega^2$

$= M_R(GM_X/2R_0) \cos^2 \theta$

- gravitational energy

$E_G = -\,2\, E_K$

- thermal and effective potential energy for the hydrostatic balance in the meridian cross section of the ring

$E_T = (5/2)\, (M_R/\mu m_H)\, kT$

$= (5/3)\, M_R(GM_X/2R_0)\, \tau \cos^{16/5} \theta$

$\tau = (3kT_0/2\mu m_H) / (GM_X/2R_0)$

- <u>total energy of the ring</u>

$E = E_K + E_G + E_T$ + (minute terms on $\theta$)

$\approx M_R(GM_X/2R_0)\, (-\cos^2\theta + 5/3\, \tau \cos^{16/5}\theta)$

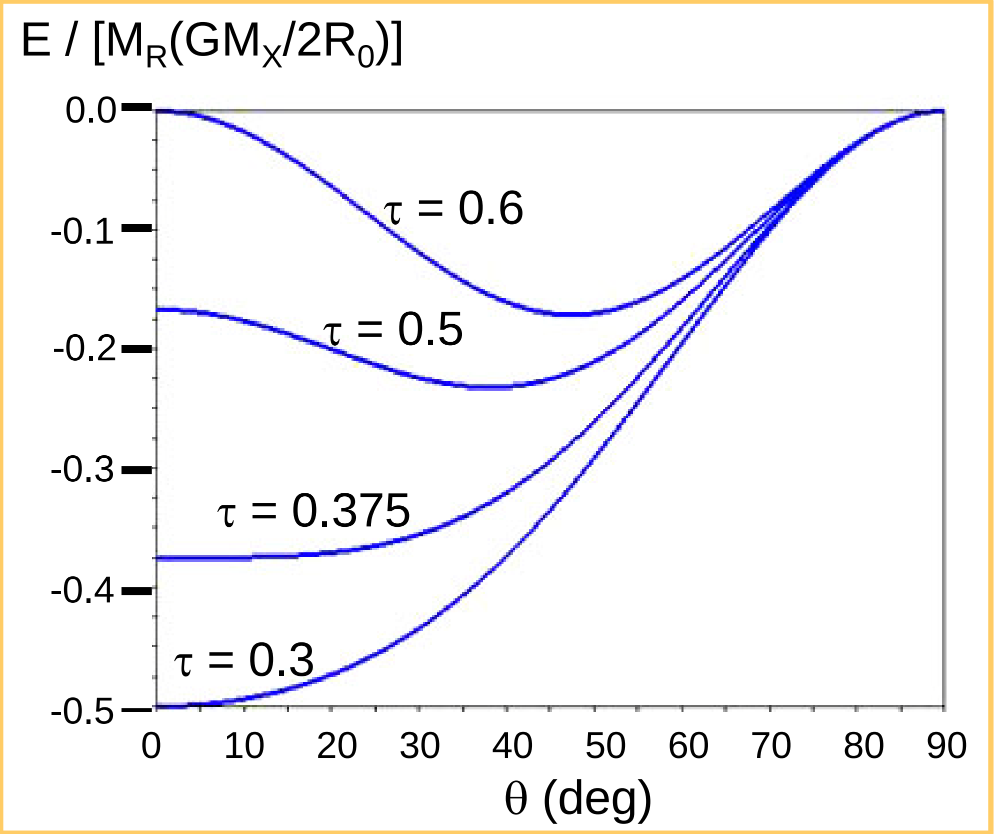


When the ring has enough thermal energy ($\tau > 3/8$), the total energy has the minimum at a certain tilt angle.

Comparison of the disk preccession scenario with observations

## Preccession periods

According to the binary motion, the tidal force torque periodically changes.

The angular velocity of the preccession periodically changes too.

$$\dot{\phi} \approx - \dot{\phi}_0 \, ( 1 + \cos 2(\dot{\phi}_0 + \Omega_B) \, t )$$

$$\Omega_B = [G(M_X+M_C) / D^3]^{1/2}$$

angular velocity of the binary motion

The average preccession angular velocity

$$\dot{\phi}_0 = (GM_C \cos \theta ) / (2D^3\Omega)$$

The preccession period

$$P_P = 2\pi / \dot{\phi}_0 = 2 \, [(M_C+M_X)/M_C] \, [\Omega/\Omega_B] \, P_B$$

a few 10 ~ a few 100 times as large as the binary period

$$P_B = 2\pi/\Omega_B$$

the binary period

- Super-orbital periodicities are observed from several binary X-ray sources.

| | binary period | super-orbital period | characteristics |
|---|---|---|---|
| Her X-1 | 1.7 days | 35 days | X-ray pulsar |
| SS433 | 13.1 days | 162.5 days | jet object |
| LMC X-4 | 1.4 days | 30 days | X-ray pulsar |
| Cyg X-1 | 5.6 days | 294 days | black hole candidate |
| LMC X-3 | 1.7 days | 198 days | black hole candidate |
| X1916-053 | 50.46 分 | ～3.8 days（？） | low mass binary |

Relation between the radius of the accretion ring (R) and the binary separation(D)

Ratio of the preccession period to the binary period

$$P_P = 2\pi / \dot{\phi}_0 = 2\,[(M_C+M_X)/M_C]\,[\Omega/\Omega_B]\,P_B$$

$$R / D = \{ 2\,[(1 + q)^{1/2}/ q]\,[P_B/P_P]\,\cos^{-1}\theta \}^{2/3} \qquad q \equiv M_C/M_X$$

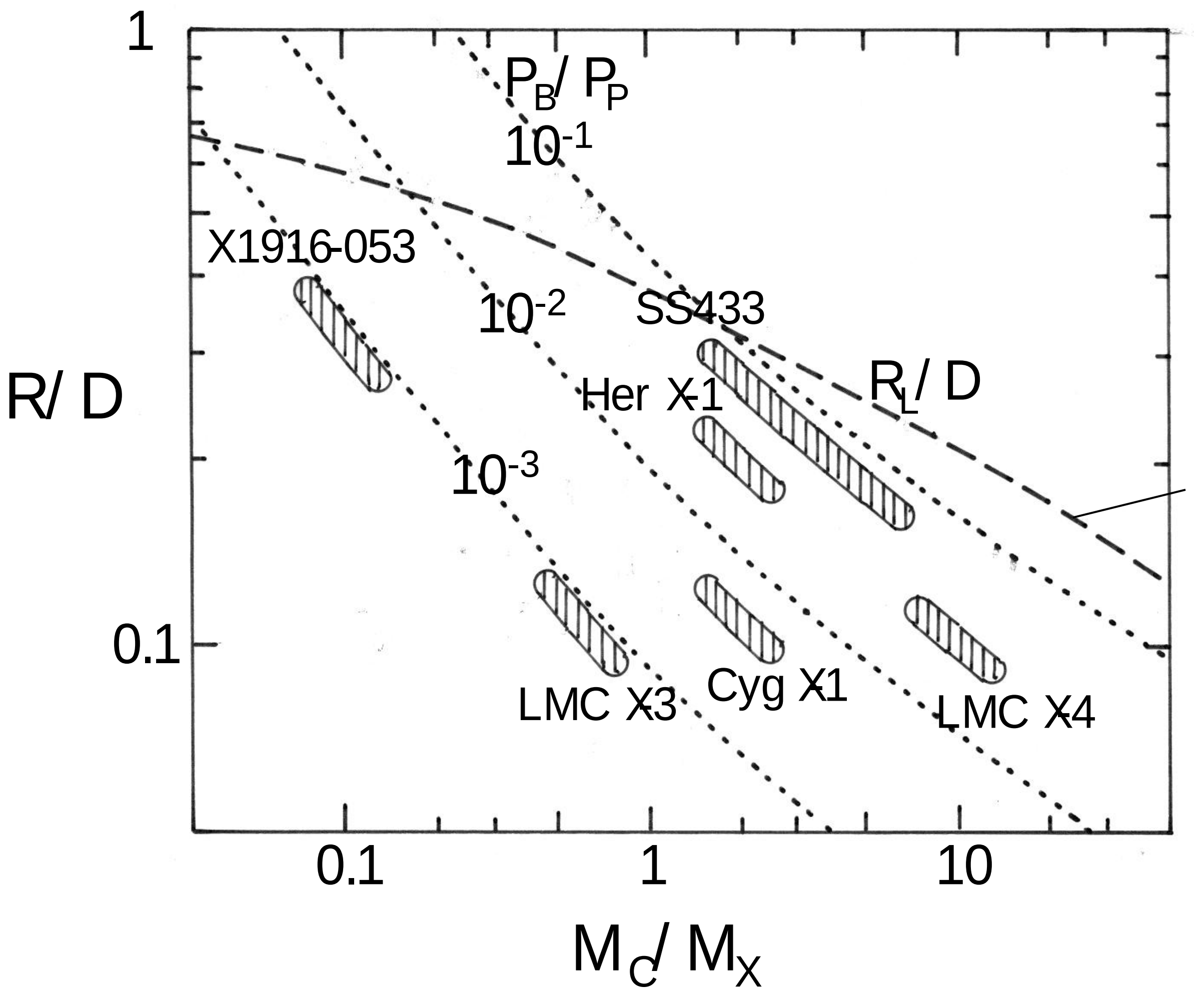


Average radius of the Roche lobe

$$R_L/D = 0.49/[0.6+q^{2/3}\ln(1+q^{-1/3})]$$

Eggeleton (1983)

# Pre-eclipse dips of Her X-1

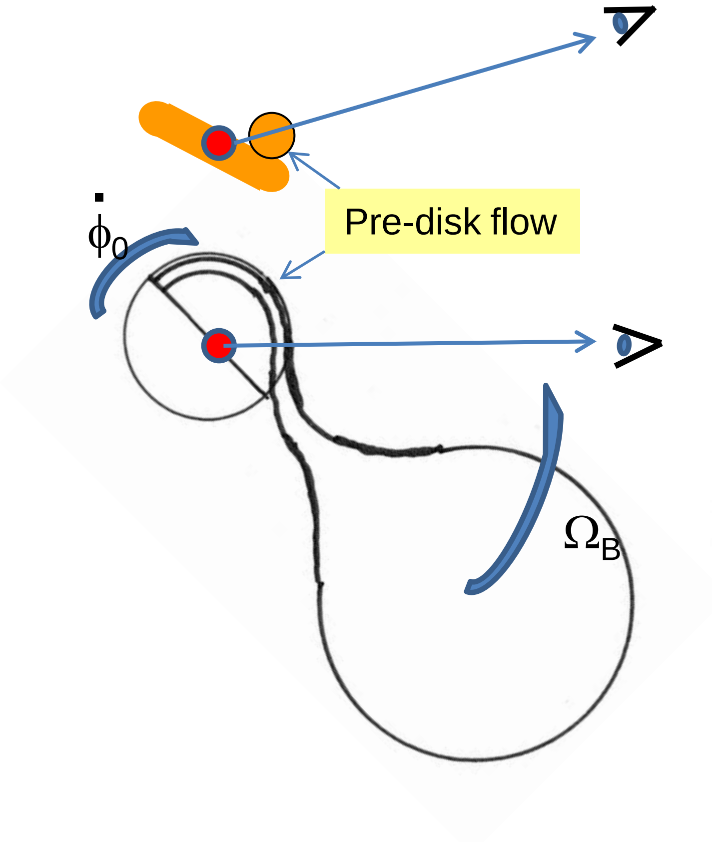


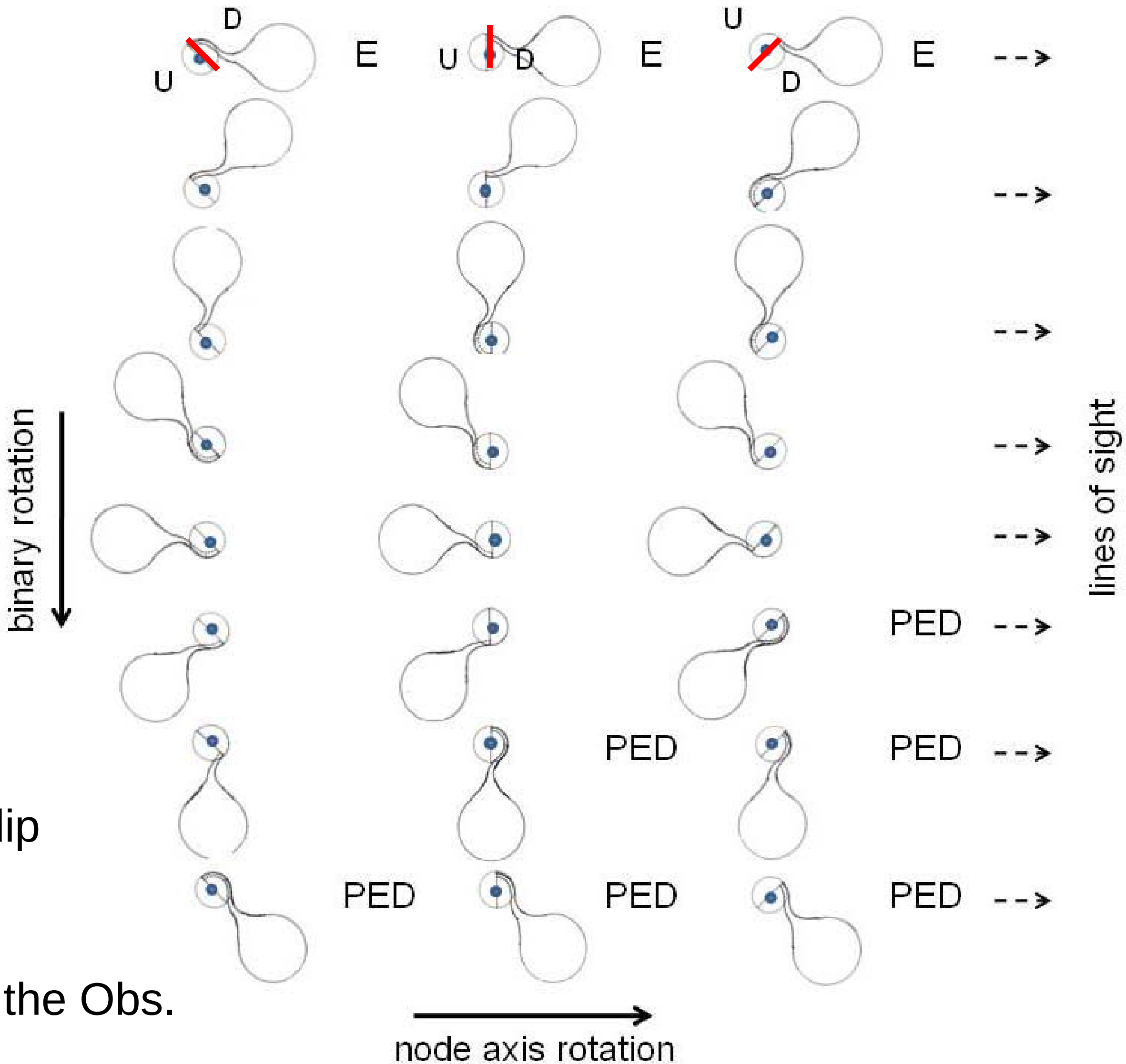


Start phase of the pre-eclipse dip

$$\dot{\phi}_B \approx - \dot{\phi}_0 - \Omega_B$$

1.62 day period : agree with the Obs.

# Nodding motion of SS433 jets

Doppler shifts due to the ring preccession

$\propto \dot{\phi} \cos \phi \propto (1 + \cos 2(\dot{\phi}_0 + \Omega_B)\, t) \cos \dot{\phi}_0 t$

$\propto \cos \dot{\phi}_0 t + (1/2) \cos (2\Omega_B + \dot{\phi}_0)\, t + (1/2) \cos (2\Omega_B + 3\dot{\phi}_0)\, t$

| | 162.5 days | 6.29 days | 5.84 days |
|---|---|---|---|
| Obs. | | 6.28 days | 5.83 days |

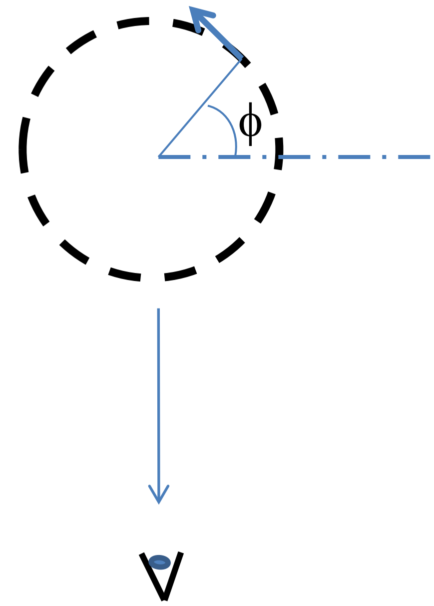


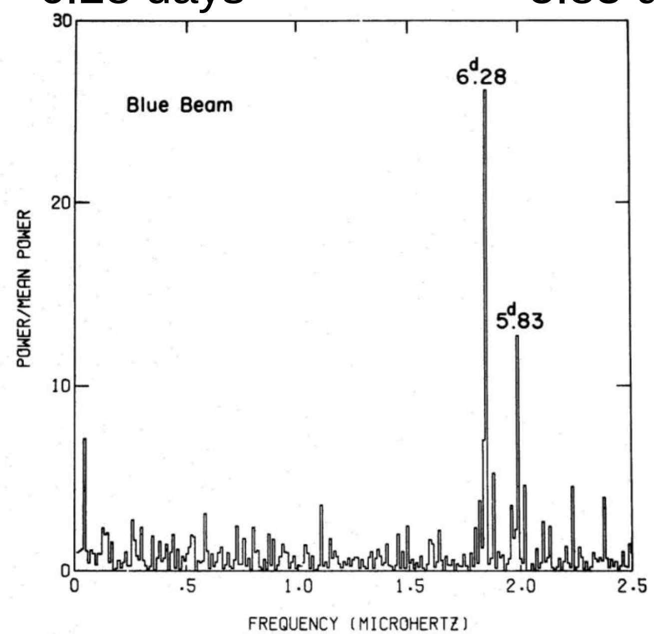


(Katz et al. 1982)

## Summary of the 1st topic

**The tidal-force induced preccession scheme can explain several observational facts quite reasonably.**

# Origin of erratic X-ray variation and seemingly broad iron line spectral feature in Seyfert galaxies

## Erratic X-ray intensity variation

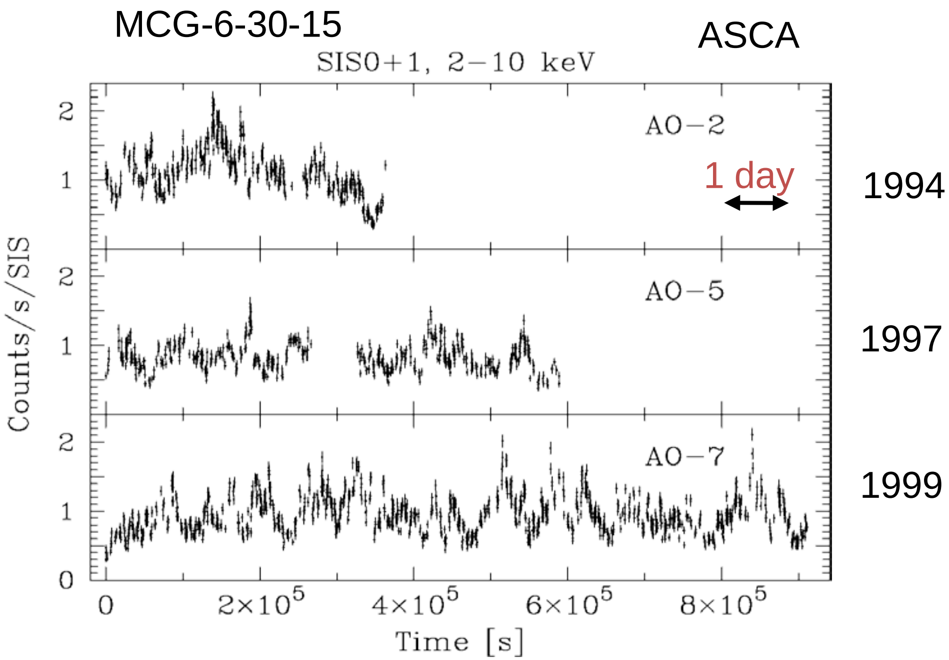


## So-called "disk-line" feature

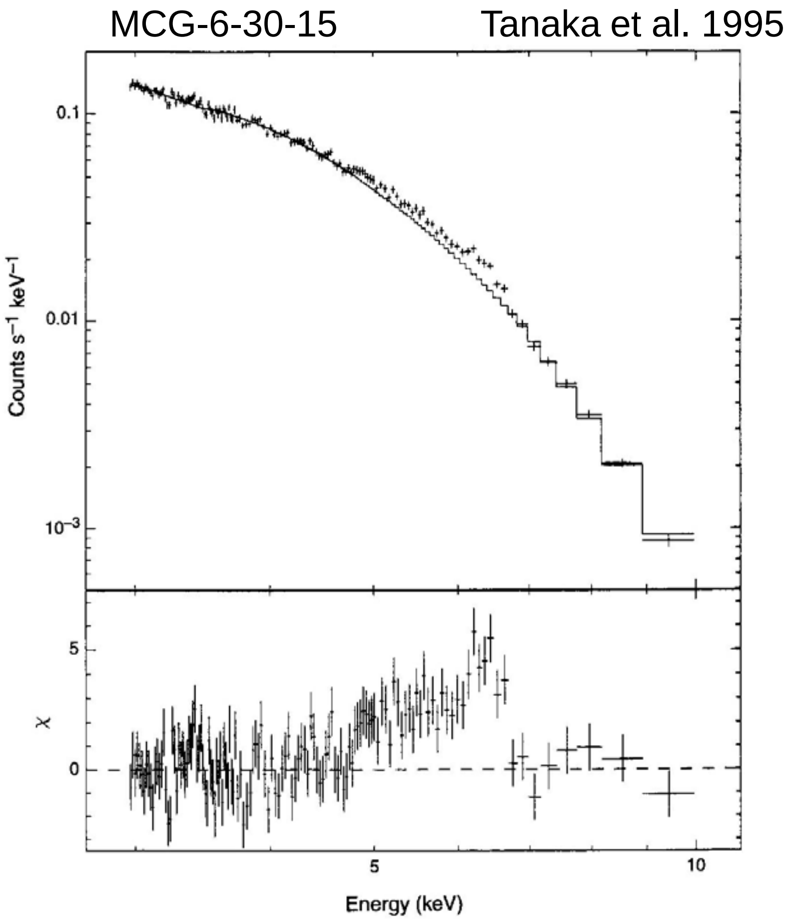

Discovery of a fluorescent iron line + a reflected component in X-ray spectra from Seyfert galaxies with Ginga (Pounds et al. 1990; Matsuoka et al. 1990)

A composite X-ray spectrum from 12 Ginga Obs. of 8 AGNs

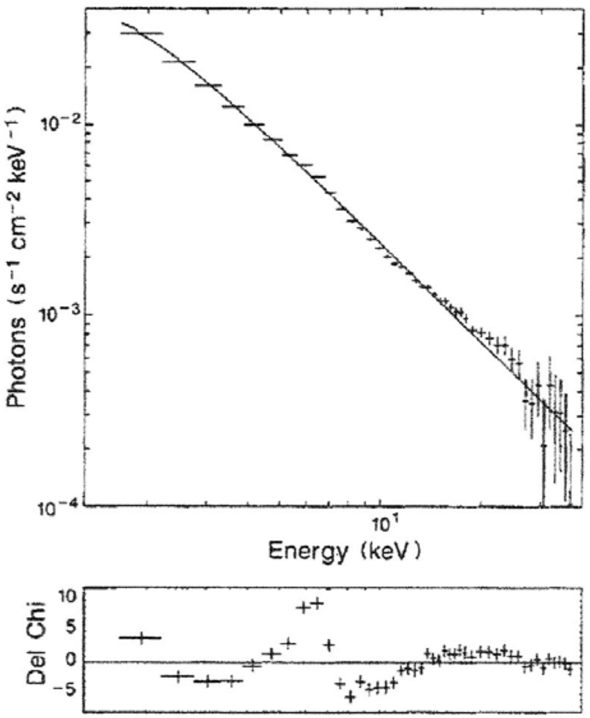


FIG. 1 Simple power-law fit to the Ginga-12 spectrum, together with a residual plot of the data minus model results.

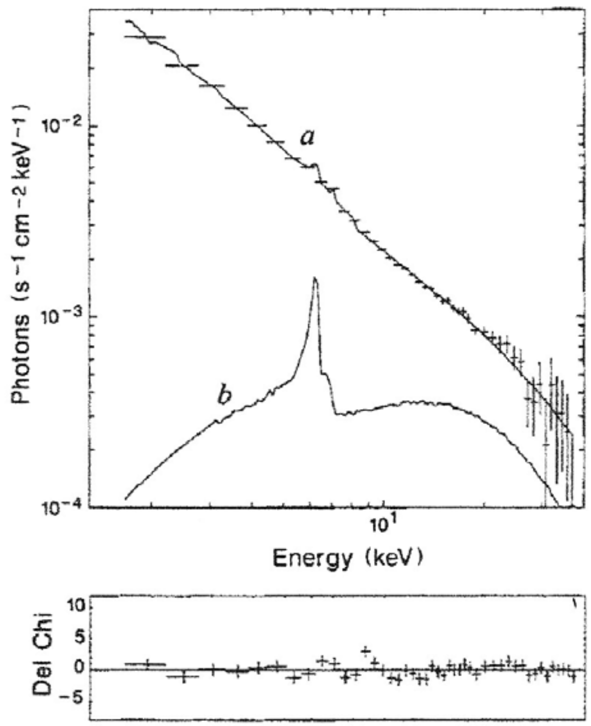


FIG. 2 *a*, Power law plus reflection and warm absorber model (as detailed in the text), together with residuals. *b*, Reflection component only.

(Pounds et al. 1990)

# X−rays reflected from Compton thick ($N_H > 10^{24}cm^{-2}$), extended ($\Omega \sim 2\pi$) cold matter

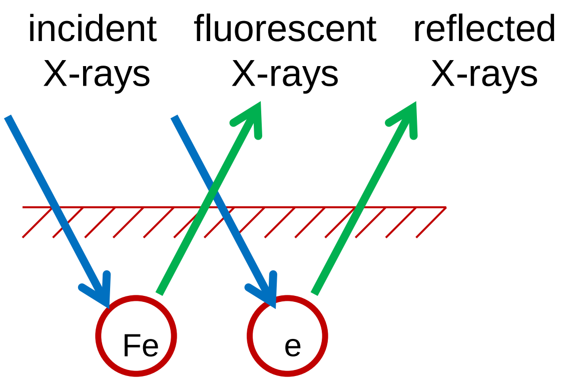


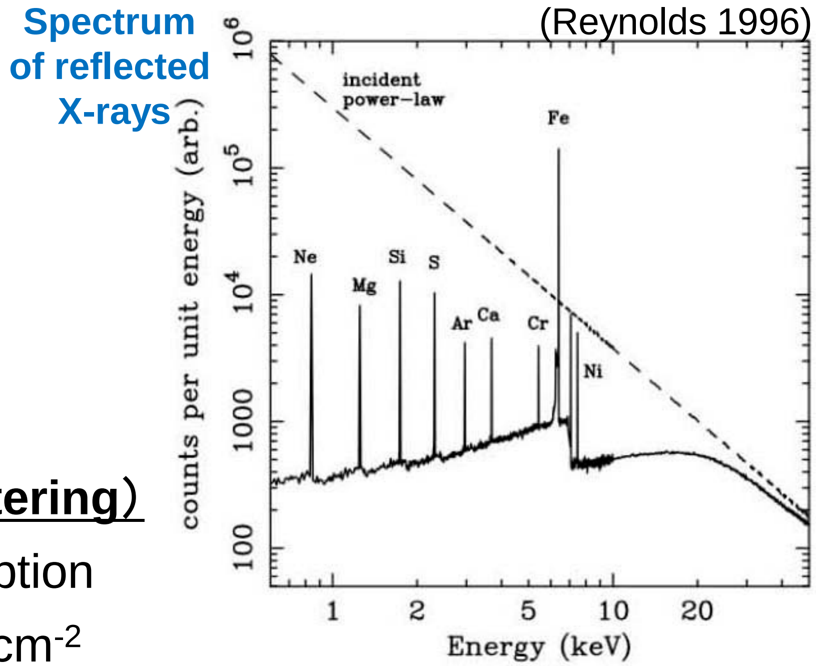


**Reflected X-rays (Compton scattering)**

continuum suffering from absorption

by matter with $N_H \sim \sigma_T^{-1} \sim 10^{24}$ cm$^{-2}$

**Fluorescent iron K-line**

equivalent width ～ 100 eV

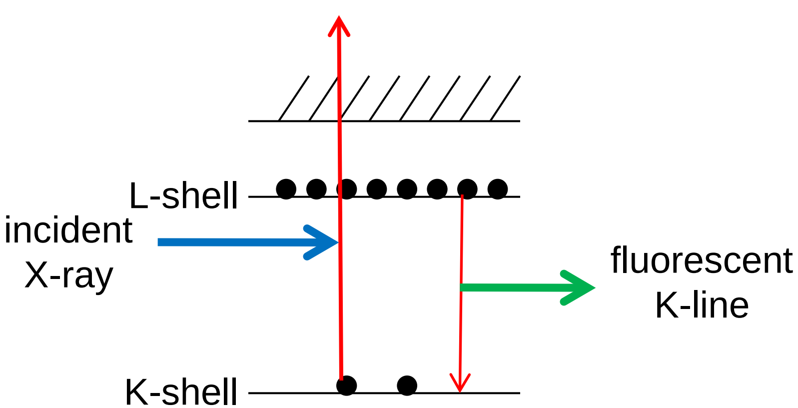


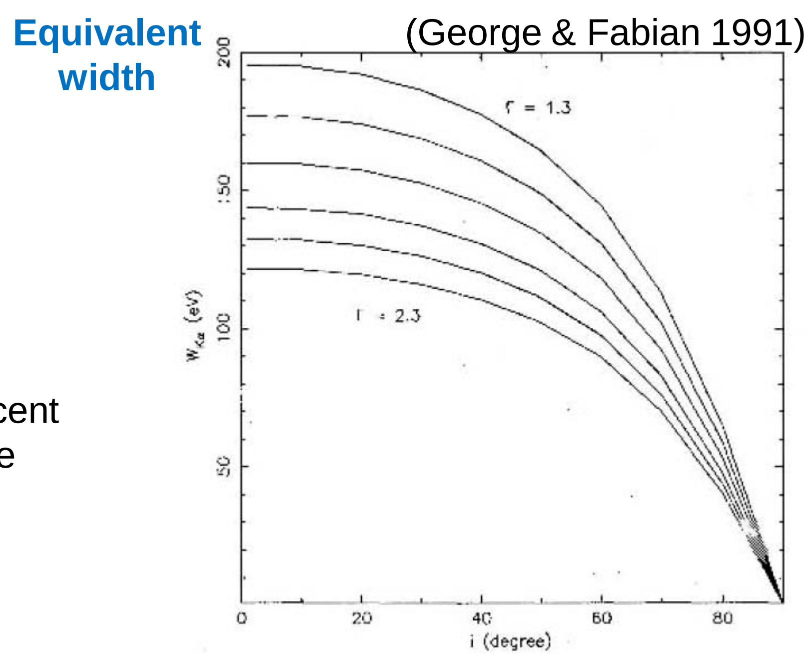

# Discovery of a very broad line-like (**“disk-line”**) feature in the X-ray spectrum of MCG-6-30-15

ASCA discovered a very broad line-like feature in the X-ray spectrum of the Seyfert galaxy, MCG-6-30-15, which is considered to be a fluorescent iron K-line from the accretion disk close to the central black hole. (Tanaka et al. 1995)

## The “disk-line” model

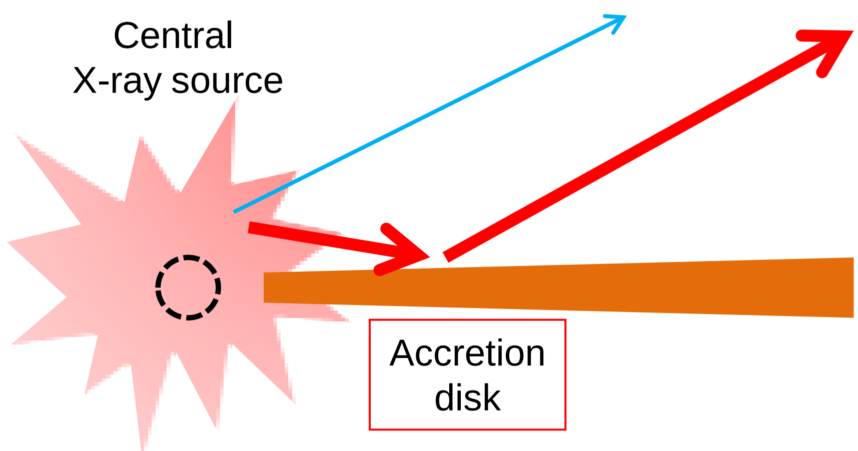


MCG-6-30-15 Tanaka et al. 1995

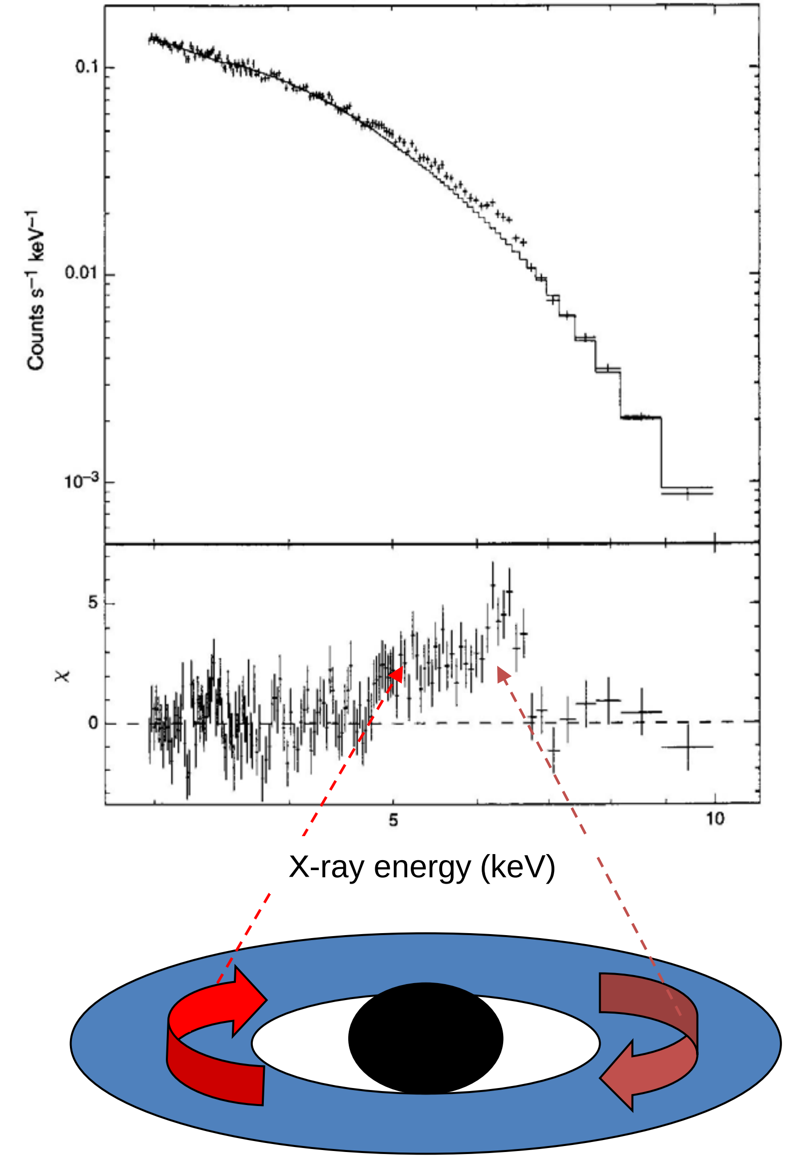

# The “disk-line” model (2-component model)

$$F(E) = N_1 P(E) + N_2 R(E)\, P(E) + I_{Disk}(E)$$

direct component

reflected component by the inner disk

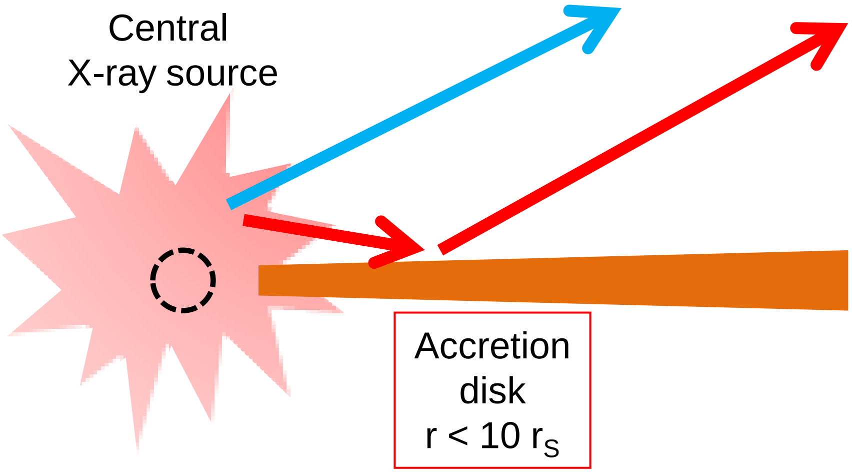


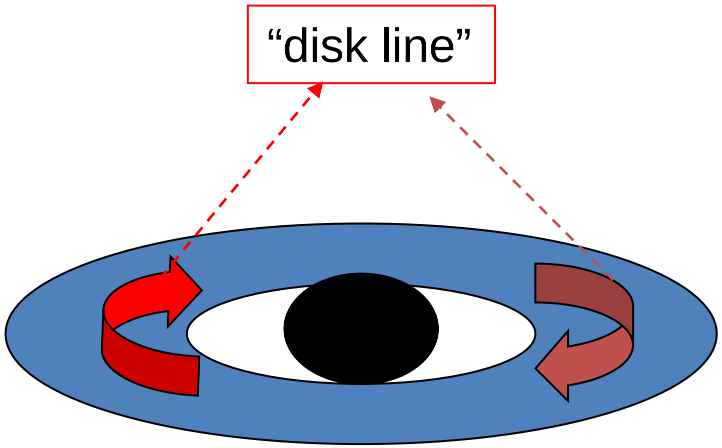


$N_1$, $N_2$ : Normalization factors of the two components.

P (E): Power law spectrum from the central X-ray source.

R(E) : Attenuation factor by reflector

$I_{Disk}(E)$ : Disk line

(Interstellar and circumstellar absorption terms are omitted for simplicity.)

# Discovery of a narrow line component

Chandra grating (HETGS) Obs. of MCG-6-30-15
(Young et al. 2005)

Iron K-line at 6.4 keV

Equivalent width ~ 20 ± 10 eV

Line width (FWHM) < 100 eV

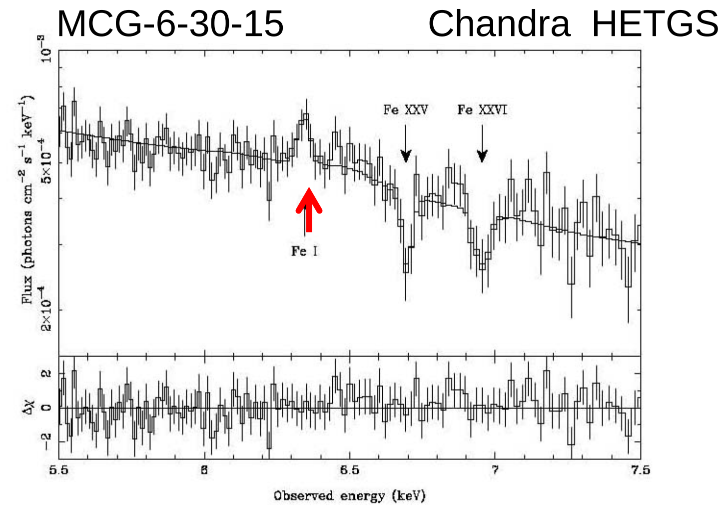


It became possible to separate the fluorescent line + reflected component from the dust torus.

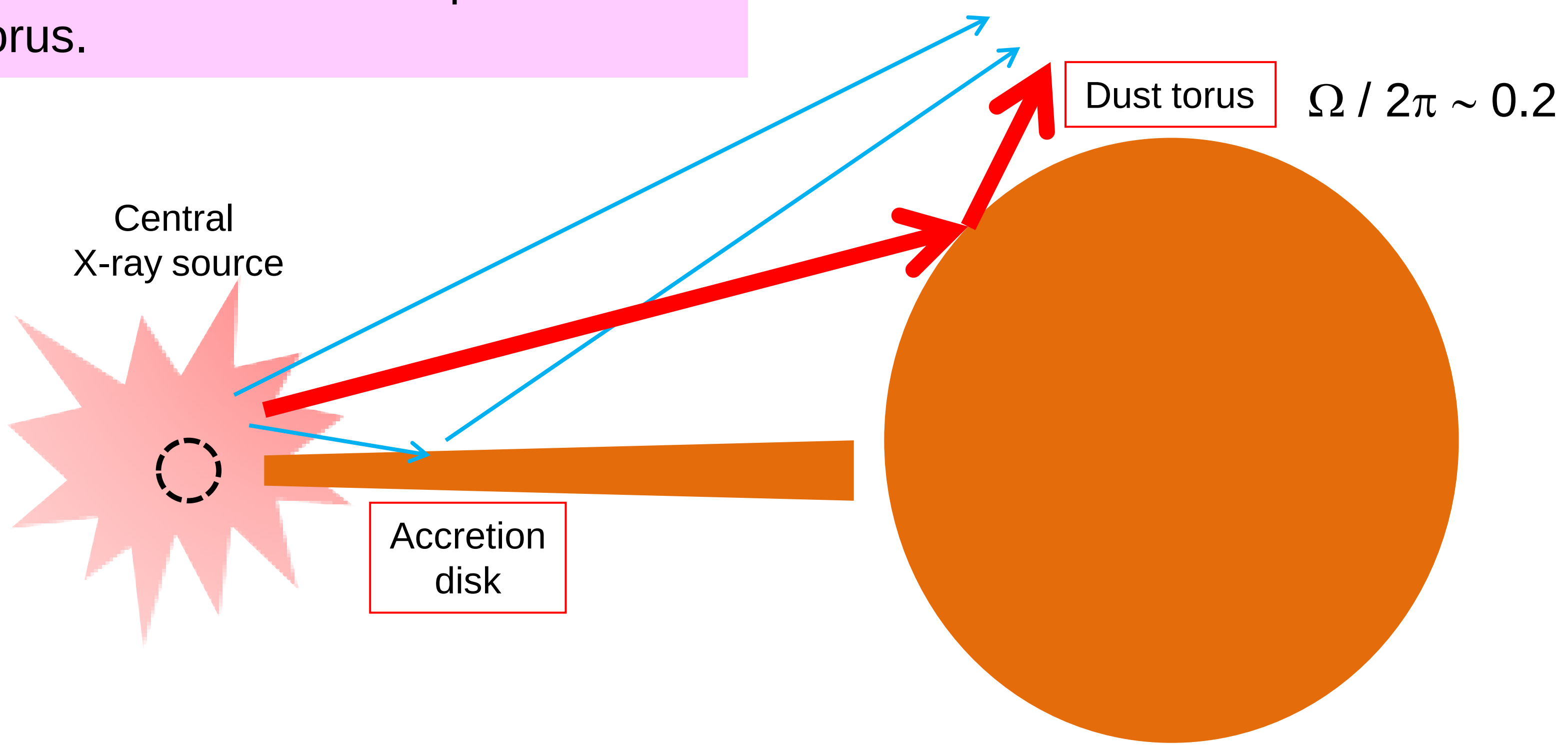

# Introduction of the 3-component model to reproduce X-ray spectra of MCG-6-30-15 observed with Suzaku

(Miyakawa, Ebisawa & Inoue 2012)

$$F(E) = \underbrace{N_1 P(E)} + \underbrace{N_2 W(E)\, P(E) + I_{Disk}(E)} + \underbrace{N_3\, R(E)\, P(E) + I_{Torus}(E)}$$

- $N_1 P(E)$: direct component
- $N_2 W(E)\, P(E) + I_{Disk}(E)$: reflected or absorbed component in the inner region
- $N_3\, R(E)\, P(E) + I_{Torus}(E)$: reflected component by the dust torus ($\Omega$ / 2$\pi$ ~ 0.2, constant in time)

$N_1$, $N_2$, $N_3$ : Normalization factors of the three components.

P (E): Power law spectrum from the central X-ray source.

W(E) : Attenuation factor by warm reflector or absorber

R(E) : Attenuation factor by cold matter

$I_{Disk}(E)$ : Disk line model (Laor 1991)

$I_{Torus}(e)$ : Narrow line at 6.4 keV

(Interstellar and circumstellar absorption terms are omitted for simplicity.)

The 3-component model

$$F(E) = N_1 P(E) + N_2 W(E)\, P(E) + I_{Disk}(E) + N_3 R(E)\, P(E) + I_{Torus}(E)$$

**Reproduces the observed spectrum in 1-40 keV quite well.**

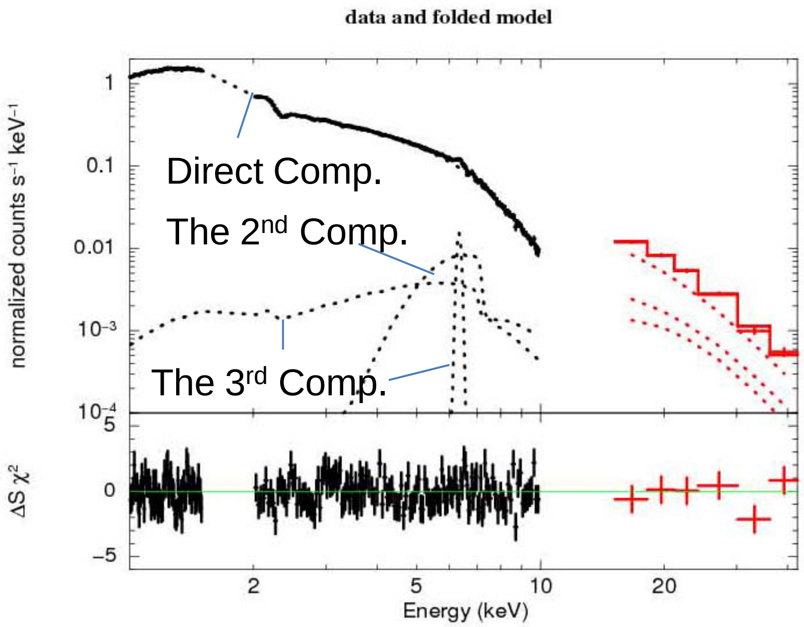


Needs no broad "disk-line" feature

$r_{in} \sim 200\ r_g$ ( > 10 $r_g$ )

Equivalent width < 40 eV

(by applying the "disk-line" model by Laor (1991))

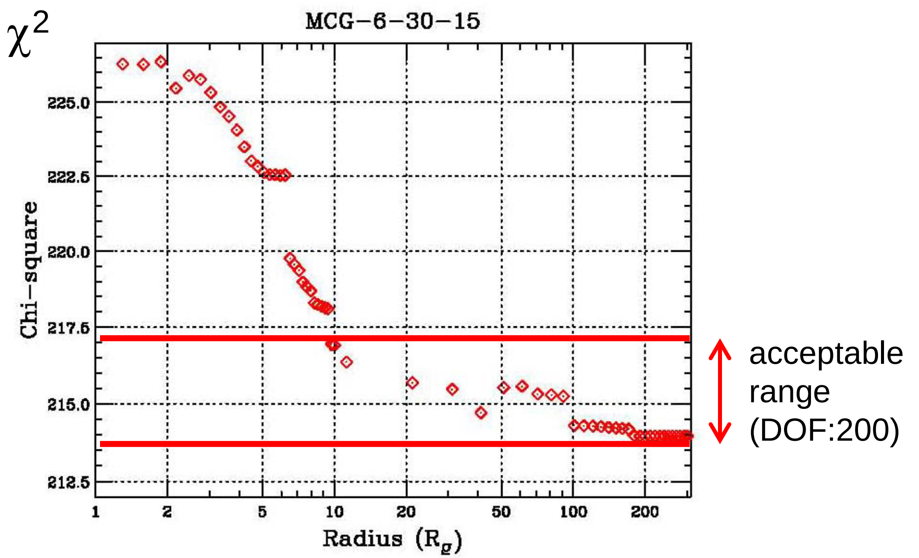

# Analyses of the time-sliced spectra in 1- 40 keV

The 3-component model was fitted to a sequence of X-ray spectrum every 20 ksec.

$$F(E) = N_1 P(E) + N_2 W(E)\,P(E) + N_3 R(E)\,P(E) + I_{Fe}(E)$$

$N_1$ and $N_2$ are treated as time-variable, while the other parameters are made the same for all the spectra. (Circumstellar absorption terms are omitted here.)

**Inverse correlation between $N_1$ and $N_2$**

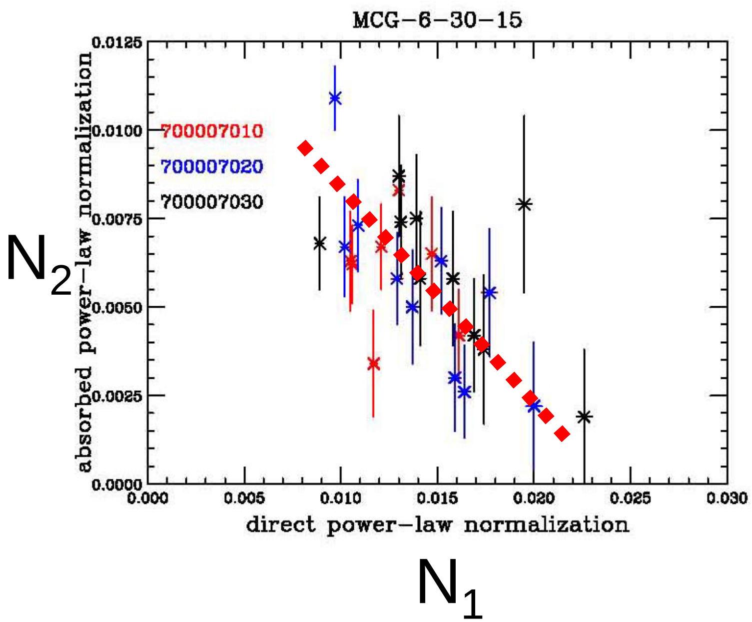


(Possibility 1) Reflection

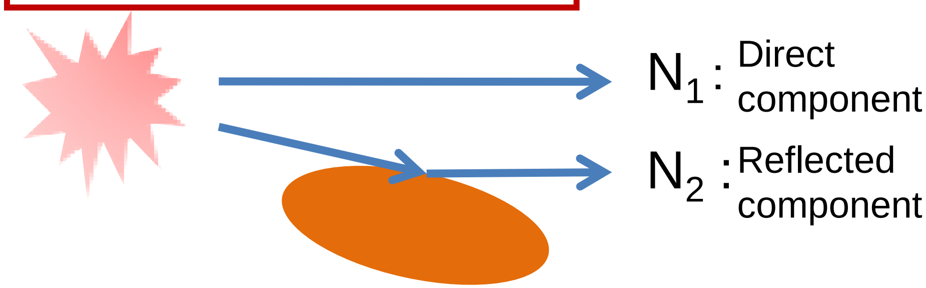


Difficult to explain the inverse correlation.

(Possibility 2) Partial absorption

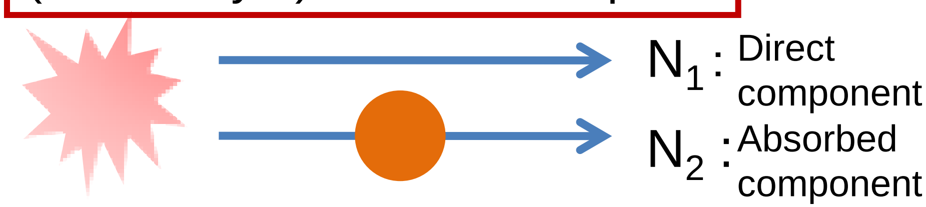


Easy to explain the inverse correlation by introducing a variable partial covering

# The variable partial covering model

| | | |
|---|---|---|
| A new normalization factor | $N = N_1 + N_2$ | are introduced. |
| A covering fraction of the absorber | $\alpha = N_2 / N$ | |

$N_1 P(E) + N_2 W(E)\, P(E)$ ➡ $N\,[(1 - \alpha) + \alpha\, W(E)]\, P(E)$

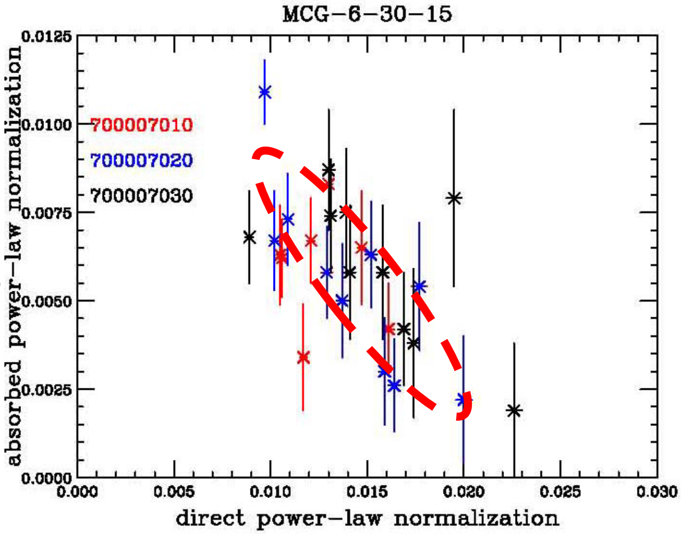


$N_2$ vs. $N_1$

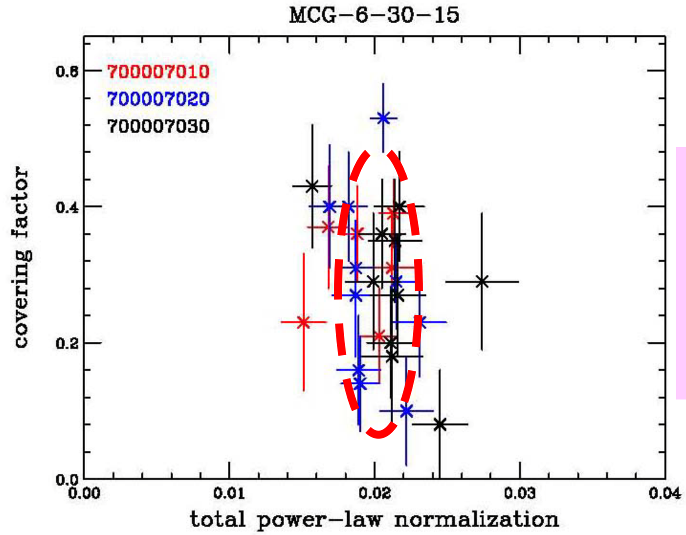


$\alpha$ vs. $N$

Much better independence between the two parameters

Difference variation function analyses (Inoue, Miyakawa & Ebisawa 2011)

$$\left(\frac{\delta F}{F}\right)^2 = \frac{(1 - W(E))^2}{[(1-\alpha) + W(E)\alpha]^2}\,\delta\alpha^2 + \left(\frac{\delta N}{N}\right)^2$$

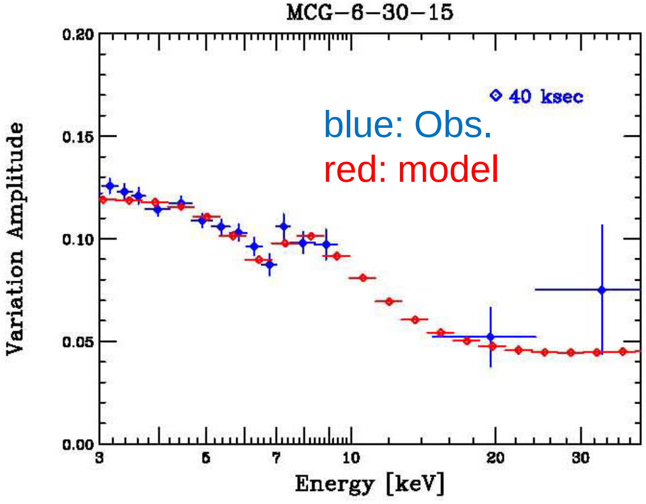


The variable partial covering model can reproduce the observed energy dependence of the variation amplitude of the X-ray flux.

# Physical considerations of the partial absorber

## Typical time-scale of the variation of $\alpha$ (the covering fraction of the absorber)

Time-scale-dependence of the variation amplitude of $\alpha$

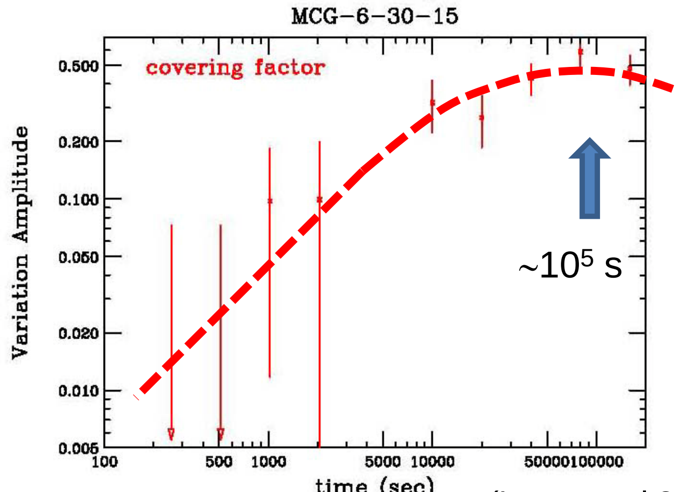


(Inoue et al.2011)

Typical time scale of the $\alpha$ variation

$\delta t \sim 10^5$ sec

Velocity of the partial absorber

$v \sim 10^9$ cm s$^{-1}$

(Typical Keplerian velocity in the BLR)

Width of the absorber

$h \sim v\,\delta t \sim 10^{14}$ cm

## Ionization degree of the absorber

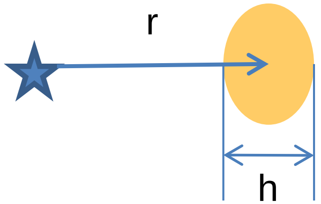


Ionization degree

$$\xi = \frac{L}{nr^2} = \frac{L}{N_H r}\left(\frac{h}{r}\right)$$

L : X-ray liminosity
n : number density
$N_H = nh$

Best fit values for the properties of the absorber

$\xi \sim 10^{1.6}$ erg cm s$^{-1}$

$N_H \sim 10^{24.2}$ cm$^{-2}$ $\sim \sigma_T^{-1}$

**<u>Distance of the partial absorbers from the central X-ray source</u>**

$r \sim 10^{15.7}$ cm

$\sim 10^3\, r_S$ (when $M_{BH} \sim 10^7\, M_{Sun}$)

**Typical distance of the broad line region**

**<u>Partial absorbers</u>**

**probably are envelopes of broad line clouds.**

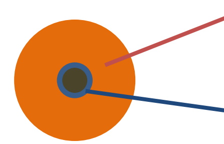

Partial absorber : $N_H \sim \sigma_T^{-1}$

Cloud core emitting optical broad lines
$N_H >> \sigma_T^{-1}$

Ebisawa et al. (2012)

applied **the variable partial covering model** to temporal and spectral variations in 2-40 keV observed from 20 more Seyfert galaxies observed with Suzaku.

## The variable partial covering model

$$F(E) = N\,(1-\alpha)\,P(E) + N\alpha W(E)\,P(E) + N_R R(E)\,P(E) + I_{Torus}(E)$$

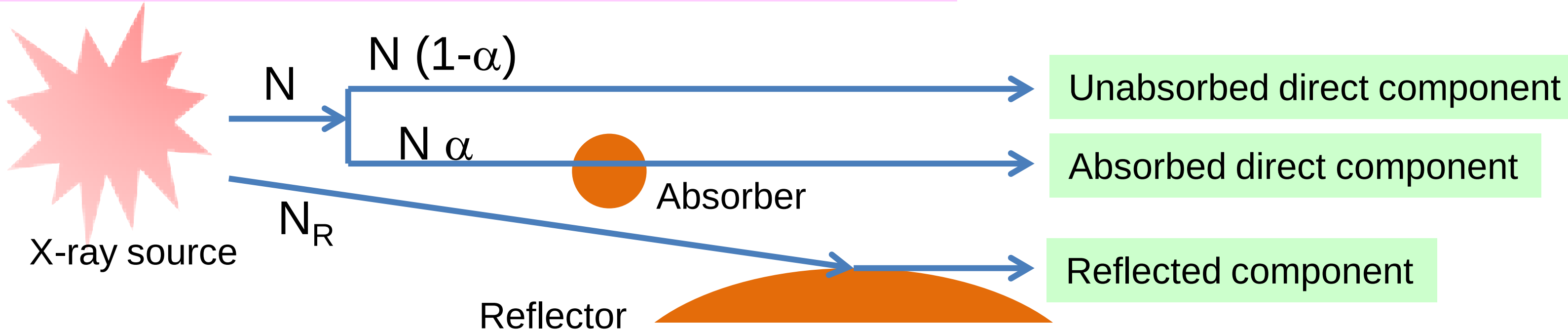


The average spectrum
intensity-sliced spectra
time-sliced spectra

} of every 21 Seyfert galaxies

are all successfully reproduced by this model !

The covering fraction of the absorber, $\alpha$, largely varies, while the normalization factor, N, of the intrinsic flux towards us is almost constant.

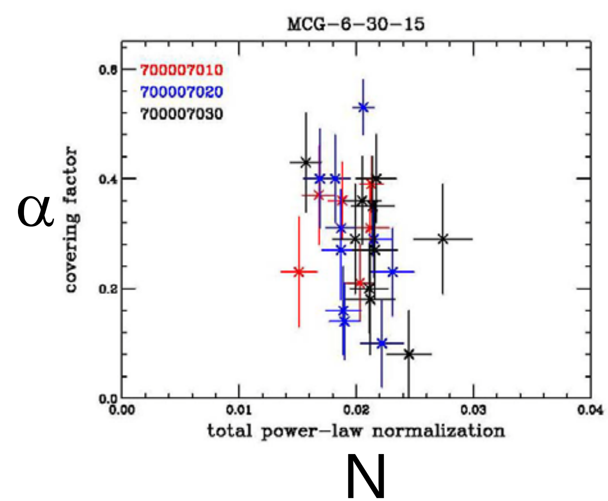

# Summary of the 2nd topic

The erratic X-ray variation and seemingly broad iron line spectral feature in Seyfert galaxies can be interpreted by the variable partial covering model.

## The variable partial covering model

$$F(E) = \underbrace{N(1-\alpha)\,P(E)}_{\text{Unabsorbed direct component}} + \underbrace{N\alpha W(E)\,P(E)}_{\text{Absorbed direct component}} + \underbrace{N_R R(E)\,P(E) + I_{Torus}(E)}_{\text{Reflected component}}$$

- X-ray variations of Seyfert galaxies are primarily explained by partial obscuration of the central X-ray source by absorbing clouds in the line of sight.
- A characteristic spectral signature around the iron K-edge in the absorbed component could be the origin of the seemingly broad iron line spectral feature (so-called “disk line” feature).